




Intrinsic nonreciprocal reflection and violation of Kirchhoff's law of radiation in planar type-I magnetic Weyl semimetal surfaces

Simo Pajovic ,* Yoichiro Tsurimaki,^{*} Xin Qian , and Gang Chen [†]

Department of Mechanical Engineering, Massachusetts Institute of Technology, Cambridge, Massachusetts 02139, USA



(Received 29 August 2020; revised 6 October 2020; accepted 9 October 2020; published 23 October 2020)

This work demonstrates that Kirchhoff's law of radiation, stating that the spectral directional emissivity and absorptivity of a surface are equal at thermal equilibrium, can be violated in planar surfaces without an external magnetic field or structures such as gratings. Modeling a type-I magnetic Weyl semimetal with an antisymmetric dielectric tensor, we show an intrinsic violation of Kirchhoff's law due to nonreciprocal surface polaritons induced by the Berry curvature and anomalous Hall velocity. This work provides a simple way to physically realize the violation of Kirchhoff's law.

DOI: [10.1103/PhysRevB.102.165417](https://doi.org/10.1103/PhysRevB.102.165417)

I. INTRODUCTION

Conventional knowledge of thermal radiation believes the spectral directional emissivity of a surface equals its spectral directional absorptivity at thermal equilibrium: $\epsilon(\omega, \theta, \phi) = \alpha(\omega, \theta, \phi)$ [1,2]. This is known as Kirchhoff's law of radiation (henceforth referred to as ‘‘Kirchhoff's law’’) and is usually thought of as a consequence of the second law of thermodynamics. In reality, Kirchhoff's law is derived assuming Lorentz reciprocity holds [1,3–5], which requires the reflectivity of the surface to be reciprocal; i.e., $\rho(\omega, \theta, \phi) = \rho(\omega, \theta, \phi + 180^\circ)$ for specular surfaces [2,6]. However, Lorentz reciprocity does not always hold, such as in magnetic systems [3,4]. By relaxing the constraint of Lorentz reciprocity, a more general form of Kirchhoff's law has been derived using thermodynamic arguments [3–5,7]:

$$\epsilon(\omega, \theta, \phi) - \alpha(\omega, \theta, \phi) = \rho(\omega, \theta, \phi) - \rho(\omega, \theta, \phi + 180^\circ). \quad (1)$$

Although most everyday surfaces are reciprocal, there is a growing interest in nonreciprocal surfaces because of their potential to experimentally violate Kirchhoff's law and enable the development of photovoltaic and thermophotovoltaic cells with efficiencies beyond the Shockley-Queisser limit [8], novel emitters and absorbers [9,10], and more compact optical switches, isolators, and circulators [11,12].

Lorentz reciprocity can be broken either by inducing a nonlinear optical response or by materials with nonsymmetric dielectric or permeability tensors ($\bar{\epsilon}^T \neq \bar{\epsilon}$, $\bar{\mu}^T \neq \bar{\mu}$, or both) [13]. Since electric and magnetic fields in most applications are not strong enough to induce nonlinear responses [14], the search for nonreciprocal systems has focused on the second condition. One way to induce an antisymmetric $\bar{\epsilon}$ is by applying a magnetic field to break time-reversal symmetry [12,13]. For example, magneto-optic materials are

known to have antisymmetric $\bar{\epsilon}$, but in order to appreciably violate Kirchhoff's law, the antisymmetric part of $\bar{\epsilon}$ must be at least the same order of magnitude as the symmetric part [15], which usually requires a large gyration vector [12]. For many magneto-optic materials, this is not the case unless a sufficient external magnetic field is applied. For example, Zhu and Fan [4] and Zhao *et al.* [16] showed via simulation that strong nonreciprocity can be achieved by applying an external magnetic field (3 and 0.3 T, respectively) to a grating structure made of InAs. However, the need for an external magnetic field makes these systems impractical for physically realizing the violation of Kirchhoff's law, although Remer *et al.* [7] were able to measure the nonreciprocal reflectivity of *n*-type InSb via attenuated total reflection for external magnetic fields up to 10 T. In fact, they recognized that this nonreciprocal reflectivity is equivalent to the violation of Kirchhoff's law via Eq. (1) and calculated the inequality between ϵ and α [7]. However, they only presented semiquantitative results for long wavelengths ($10^2 - 10^3 \mu\text{m}$), which are less relevant to thermal applications, and did not discuss the connection between Kirchhoff's law and Lorentz reciprocity in general nor suggest a detailed physical explanation of the nonreciprocity and resulting violation of Kirchhoff's law.

One approach not requiring an external magnetic field is to use materials exhibiting the anomalous Hall effect (AHE), which can result in naturally large off-diagonal components of $\bar{\epsilon}$ [17]. In particular, magnetic Weyl semimetals (WSMs) are a class of materials that has attracted great attention as a candidate for violating Kirchhoff's law due to their time-reversal symmetry breaking and large AHE. For example, $\text{Co}_3\text{Sn}_2\text{S}_2$, a confirmed [18] type-I magnetic WSM, has a measured anomalous Hall angle of 20% [19], which leads to large off-diagonal components of $\bar{\epsilon}$ [5]. The large AHE of magnetic WSMs results from the momentum space interaction between the Berry curvature Ω_n of electrons and an external electric field E . The electronic band structure of WSMs is characterized by pairs of ‘‘band touching points’’ of opposite chirality in momentum space, called Weyl nodes, which behave as sources and sinks of Berry curvature [20]. The separation between a

*These authors contributed equally to this work.

[†]gchen2@mit.edu

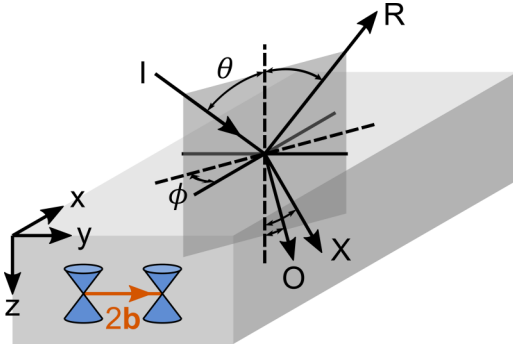


FIG. 1. Schematic of the air-Weyl semimetal (WSM) reflection configuration. The linearly polarized incident wave I strikes the surface of the WSM with Weyl node separation $2b$ at polar and azimuthal angles of incidence θ and ϕ , respectively, producing a reflected wave R and two transmitted waves O (ordinary wave) and X (extraordinary wave).

pair of Weyl nodes, $2b$, points in the same direction as the Berry curvature (from source to sink). Under the influence of \mathbf{E} , electrons, collectively excited as Weyl fermions [20], experience an anomalous Hall velocity orthogonal to $\mathbf{\Omega}_n$ and \mathbf{E} : $\mathbf{v}_{AHE} \sim \mathbf{E} \times \mathbf{\Omega}_n$. This is known as the intrinsic mechanism of the AHE [17] and plays an important role in nonreciprocity in magnetic WSMs. In fact, the optical anisotropy [21,22] and gyrotropy [21–25] of magnetic WSMs as well as their nonreciprocity [22,23] as a result of their large AHE have been recognized. Recently, Zhao *et al.* [15] and Tsurimaki *et al.* [5] showed via simulation that magnetic WSMs can be used with grating structures to achieve strong nonreciprocity and violation of Kirchhoff's law without an external magnetic field.

Here, we show that nonreciprocal reflectivity can be achieved using a planar interface between a type-I magnetic WSM and air without the need for an external magnetic field or surface structuring (e.g., gratings like in previous studies). Our work highlights the intrinsic nonreciprocal nature of magnetic WSMs due to their Berry curvature-induced AHE. We also suggest a physical explanation linking the Berry curvature-induced AHE to the existence of nonreciprocal surface polaritons, which in turn manifest in the nonreciprocal reflectivity. The ability to achieve nonreciprocity without an external magnetic field and surface structuring opens up opportunities to experimentally demonstrate the violation of Kirchhoff's law and for compact nonreciprocal devices.

II. AIR-WEYL SEMIMETAL REFLECTIVITY MODEL

Figure 1 shows the WSM surface under study. An s - or p -polarized plane wave I of angular frequency ω propagates at polar and azimuthal angles of incidence θ and ϕ , with wave vector $\mathbf{k} = (\omega/c)\mathbf{s}$ in air (refractive index $n = 1$), where $\mathbf{s} = [\sin\theta \cos\phi, \sin\theta \sin\phi, \cos\theta]^T$. At the air-WSM interface, the incident wave produces a reflected wave R and two transmitted waves O and X , corresponding to ordinary and extraordinary modes. In this work, we use the model of the bulk dielectric tensor of a type-I magnetic Weyl semimetal derived by Chen *et al.* [21] and built upon in our previous

study [5]. For a WSM with one pair of Weyl nodes separated in the y direction (k_y direction in momentum space), as shown in Fig. 1, the bulk dielectric tensor is

$$\bar{\bar{\epsilon}}(\omega) = \begin{bmatrix} \epsilon_{xx} & 0 & ig \\ 0 & \epsilon_{yy} & 0 \\ -ig & 0 & \epsilon_{zz} \end{bmatrix}. \quad (2)$$

In Eq. (2), $g = \sigma_{yz}(\omega)/\epsilon_0\omega$ represents the contribution to $\bar{\bar{\epsilon}}$ from the AHE [5], where $\sigma_{yz}(\omega)$ is the yz component of the bulk optical conductivity and ϵ_0 is the permittivity of free space. The diagonal terms are given by $\epsilon_{nm}(\omega) = \epsilon_\infty + i\frac{\sigma_{nm}(\omega)}{\epsilon_0\omega}$, where ϵ_∞ is the background dielectric constant, $\sigma_{nm}(\omega)$ is the directional bulk optical conductivity, and $n = x, y, z$. We also take $\mu = 1$, which is a common approximation for magneto-optic materials [13,26]. There are six parameters determining $\bar{\bar{\epsilon}}(\omega)$ [21]: the Weyl node separation $2b = 2|\mathbf{b}|$, the Fermi velocity v_F , the Fermi energy E_F , the damping factors due to bulk Weyl fermions γ_b and Fermi arc surface states γ_s , and the background dielectric constant ϵ_∞ . We chose the same parameters as in our previous work [5] but briefly summarize our justifications for choosing them here. We chose $2b = 0.45 \text{ \AA}^{-1}$, which is close to reported values for $\text{Co}_3\text{Sn}_2\text{S}_2$ (0.3 \AA^{-1}) [27] and Mn_3Sn ($0.5\text{--}1 \text{ \AA}^{-1}$) [28]. We chose $v_F = 1 \times 10^5 \text{ m/s}$ and $E_F = 60 \text{ meV}$, which are independent in this model. This is in line with predicted values for $\text{Co}_3\text{Sn}_2\text{S}_3$ ($E_F = 60 \text{ meV}$) [19], Co_2MnGa ($E_F = 80 \text{ meV}$) [29], $\text{Y}_2\text{Ir}_2\text{O}_7$ ($v_F = 2 \times 10^5 \text{ m/s}$) [30], and Mn_3Sn ($E_F \sim 50 \text{ meV}$) [28]. Paralleling Chen *et al.* [21] and our previous study [5], we chose $\gamma_b = \gamma_s = 15 \text{ meV}$ as a representative value since these are generally more difficult to estimate and depend on the types of interactions and disorder present in the WSM being modeled. Lastly, we chose $\epsilon_\infty = 10$, which is the same order of magnitude as the background dielectric constant in $\text{Eu}_2\text{Ir}_2\text{O}_7$ ($\epsilon_\infty = 13$) [31]. The real and imaginary parts of the components of $\bar{\bar{\epsilon}}(\omega)$ (i.e., ϵ_{xx} , ϵ_{yy} , ϵ_{zz} , and g) are plotted in Figs. 2(a) and 2(b), respectively.

We calculate the reflectivity using a simplified version of the Berreman 4×4 matrix method [32] derived by Abdulhalim [33]. This method exactly calculates the reflection matrix between two media with arbitrary dielectric tensors, as long as the tangential components of the electric and magnetic fields are continuous: $E_{\parallel}|_{z=0^+} = E_{\parallel}|_{z=0^-}$ and $H_{\parallel}|_{z=0^+} = H_{\parallel}|_{z=0^-}$ [33]. Although type-I magnetic WSMs can host Fermi arc surface states, which would introduce surface dipole layer and surface current terms in the electric and magnetic field boundary conditions, respectively [21], in our previous work, we showed that such states do not significantly affect the optical response for the bulk dielectric tensor we used in our models [5]. Under these conditions, the reflection matrix in the (p, s) polarization basis is given by

$$\begin{bmatrix} r_{p,p} & r_{p,s} \\ r_{s,p} & r_{s,s} \end{bmatrix} = T^{-1} (E_{12n}^{-1} E_{34m} - H_{12n}^{-1} H_{34m})^{-1} \times (H_{12n}^{-1} H_{12m} - E_{12n}^{-1} E_{12m}) T, \quad (3)$$

where $E_{ijl} = (V_{ei}U_{ej})_l$ and $H_{ijl} = (V_{hi}U_{hj})_l$; $i, j = 1, 2, 3, 4$ denote propagation modes—i.e., 1 = forward-propagating O wave, 2 = forward-propagating X wave, 3 = backward-propagating O wave, and 4 = backward-propagating X wave

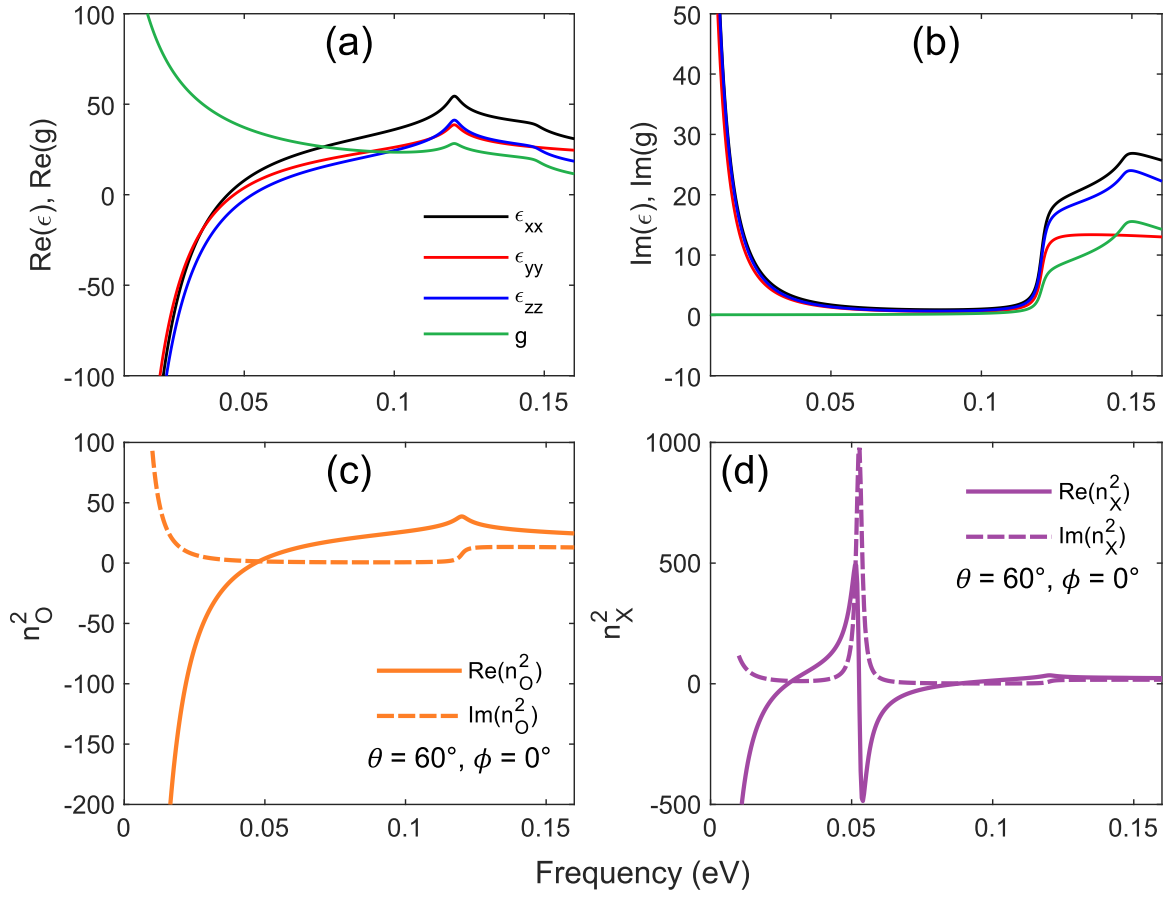


FIG. 2. (a) Real and (b) imaginary parts of the components of the bulk dielectric tensor of the Weyl semimetal (WSM). Bulk plasmon dispersion of (c) ordinary (O) and (d) extraordinary (X) modes supported by the WSM, plotted as the real and imaginary parts of the effective index of refraction squared of each mode for $\theta = 60^\circ$ and $\phi = 0^\circ$.

(in air, the 3 and 4 wave vectors are degenerate). The subscript $l = m, n$ denotes the lower ($m, z < 0$) or upper ($n, z > 0$) medium, $V_{e,h}$ and $U_{e,h}$ are eigenvectors of the electromagnetic wave equation corresponding to the electric (e) and magnetic (h) fields, and T is a transformation matrix that rotates the x - and y directions to coincide with the p - and s -polarization directions. If medium m is air, $E_{12m} = E_{34m} = \mathbb{I}$, where \mathbb{I} is the identity matrix, and $H_{12m} = -H_{34m}$. Finally, the reflectivities of s - and p -polarized light are $\rho_s = |r_{s,s}|^2 + |r_{s,p}|^2$ and $\rho_p = |r_{p,p}|^2 + |r_{p,s}|^2$, respectively, where the reflection coefficient subscripts denote the polarizations of the incident and reflected waves in that order. Details on this method can be found in Appendix A.

III. RESULTS AND DISCUSSION

A. Reflectivity of s - and p -polarized light

We investigated ρ_s and ρ_p and emphasize two limiting cases: the Voigt configuration (propagation normal to \mathbf{b} , $\phi = 0^\circ, 180^\circ$), which is nonreciprocal for p -polarized waves and has been used in studies on the violation of Kirchhoff's law [4,5,15], and the Faraday configuration (propagation parallel to \mathbf{b} , $\phi = 90^\circ, 270^\circ$), which is reciprocal for both polarizations [5,15,34,35]. Thus, we focus here on p -polarized waves, although results on s -polarized waves will be briefly discussed

at the end of this section. Figure 3(a) shows plots of ρ_p as a function of ω and ϕ at $\theta = 60^\circ$. At $\phi = 0^\circ$ and 180° , the WSM exhibits a Drude-like response at lower frequencies [21] and a Lorentzian response at higher frequencies (a peak followed by a falling edge in the reflectivity). This parallels the bulk plasmon dispersion of X waves, plotted in Fig. 2(d), which are p -polarized and thus couple to p -polarized incident waves. The nonreciprocity in the Voigt configuration is clear: ρ_p at $\phi = 0^\circ$ and 180° are not identical, and furthermore, the largest nonreciprocity, expressed as $\rho_p(\omega, \theta, \phi) - \rho_p(\omega, \theta, \phi + 180^\circ)$, is at the approximate frequencies 0.028 and 0.088 eV, at which there are reflectivity falling edges. The nonreciprocity can also be seen in the analytical equations for the reflection coefficients in the Voigt configuration (see Appendix A). By contrast, at $\phi = 90^\circ$ and 270° (not shown but identical to 90°), the reflectivity is reciprocal with only one falling edge at approximately 0.046 eV.

The physical significance of the reflectivity falling edges and their nonreciprocity is linked to the surface polaritons (SPs) supported by the WSM. Whereas the bulk plasmon dispersion [Figs. 2(c) and 2(d)] is strictly reciprocal [36], WSMs are known to support surface plasmon polaritons whose dispersion is nonreciprocal in the Voigt configuration and reciprocal in the Faraday configuration [34,37]. Physically, this can be understood via the AHE and arguments similar to those in Ref. [38] explaining the chirality of Berry

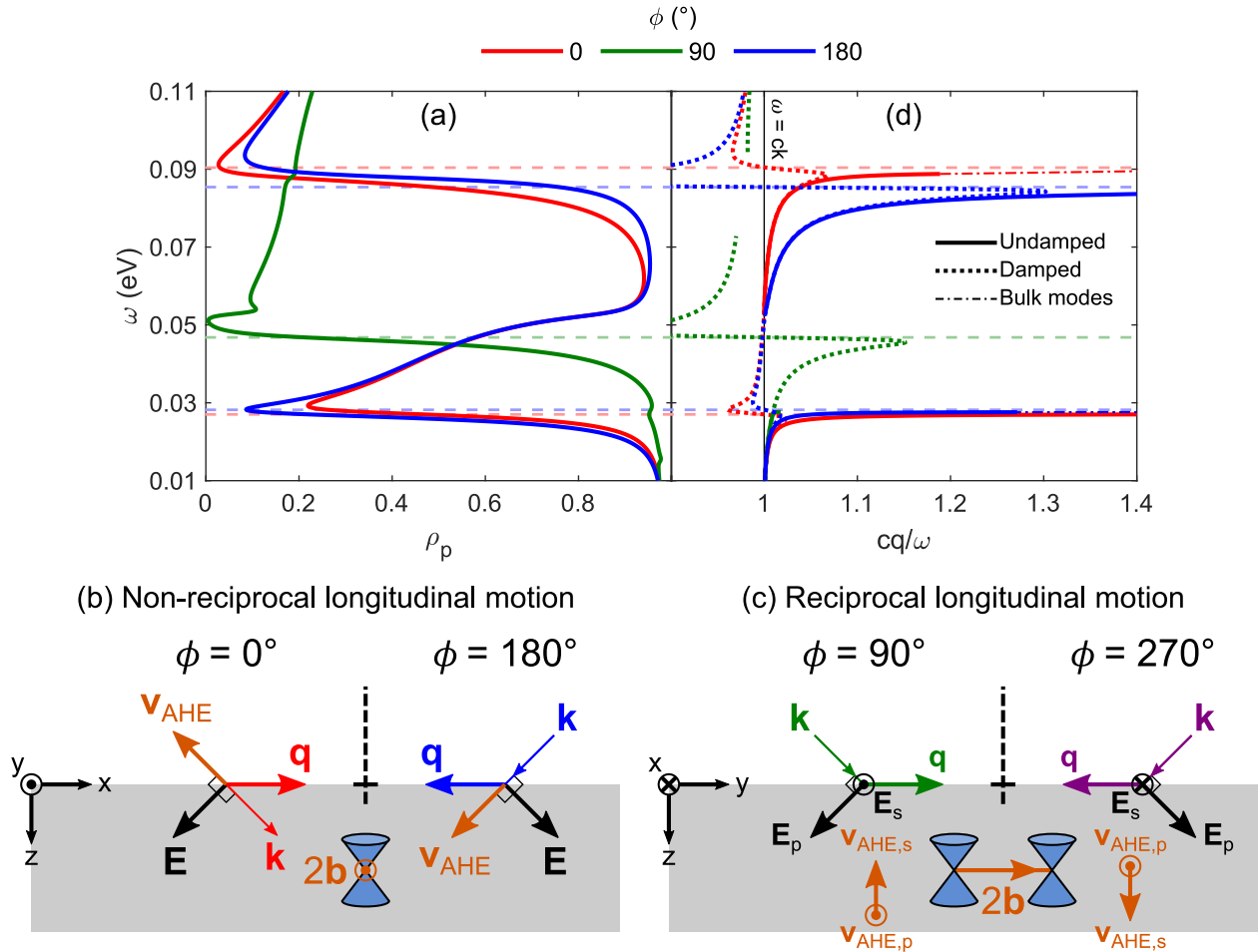


FIG. 3. (Counterclockwise) (a) Reflectivity of p -polarized waves ρ_p as a function of the frequency ω and azimuthal angle of incidence ϕ at a polar angle of incidence $\theta = 60^\circ$ for $\phi = 0^\circ$ (red, forward-propagating Voigt configuration), 90° (green, Faraday configuration), and 180° (blue, backward-propagating Voigt configuration). (b) Schematic explaining the nonreciprocity of surface polaritons (SPs) in the Voigt configuration. The electric field of a p -polarized incident wave \mathbf{E} creates an anomalous Hall velocity \mathbf{v}_{AHE} orthogonal to \mathbf{E} and \mathbf{b} . \mathbf{v}_{AHE} changes the velocity of Weyl fermions in the longitudinal (\mathbf{q}) direction, creating nonreciprocal SPs. (c) Reciprocity of SPs in the Faraday configuration. \mathbf{v}_{AHE} is normal to \mathbf{q} and does not affect the longitudinal motion of Weyl fermions. (d) Undamped and damped SP dispersions in the same directions as the reflectivity, with matching colors. The dotted lines are the frequencies where the damped SP dispersion intersects the light line, $\omega = ck$. Only the real parts of the damped SP dispersions are shown.

plasmons. Since $\mathbf{v}_{AHE} \sim \mathbf{E} \times \boldsymbol{\Omega}_n$ and $\boldsymbol{\Omega}_n$ points in the y direction (parallel to $2\mathbf{b}$), \mathbf{v}_{AHE} is restricted to the xz plane (as implied by the off-diagonal components of $\bar{\epsilon}$). Since SPs are restricted to the xy plane, only those propagating along the x axis can be influenced by the AHE. Figure 3(b) shows the direction of \mathbf{v}_{AHE} for p -polarized incident waves in the Voigt configuration. Treating the charge carriers as semiclassical wave packets of Weyl fermions, at $\phi = 0^\circ$, \mathbf{v}_{AHE} retards each Weyl fermion moving in the \mathbf{q} direction (where \mathbf{q} is the SP in-plane wave vector). At $\phi = 180^\circ$, \mathbf{v}_{AHE} accelerates each Weyl fermion moving in the \mathbf{q} direction. Clearly, the effect of \mathbf{v}_{AHE} on the longitudinal motion of Weyl fermions depends on \mathbf{q} . Collectively, \mathbf{v}_{AHE} should affect the propagation of SPs, which consist of Weyl fermions excited by the incident wave. Since the effect of \mathbf{v}_{AHE} on the Weyl fermions and thus the SPs is different in opposing directions, the SPs are nonreciprocal in the Voigt configuration. In the absence of the AHE, Weyl fermions would not feel a direction-dependent influence at all,

so the SPs would be reciprocal. In the Faraday configuration, shown in Fig. 3(c), $\mathbf{v}_{AHE,s}$ and $\mathbf{v}_{AHE,p}$, created by s - and p -polarized incident waves, respectively, are both normal to \mathbf{q} and do not affect the longitudinal motion of Weyl fermions. As a result, the SPs are reciprocal in the Faraday configuration.

The SP dispersions in both configurations are derived in Appendix B and plotted in Fig. 3(d), agreeing with the conclusions of our physical arguments. The WSM hosts two nonreciprocal SPs in the Voigt configuration and one reciprocal SP in the Faraday configuration, similar to magnetoplasmons in n -type InSb [39]. The reflectivity falling edges match the frequencies at which the damped SP dispersions intersect the light line, indicated by the colored dashed lines. This indicates coupling between incident waves and SPs [7].

We remark that in between the Voigt and Faraday configurations, s -polarized waves are nonreciprocal, as can be seen in Fig. 4(a), which shows plots of ρ_s as a function of ω and ϕ at $\theta = 60^\circ$. At ϕ values in between the limiting

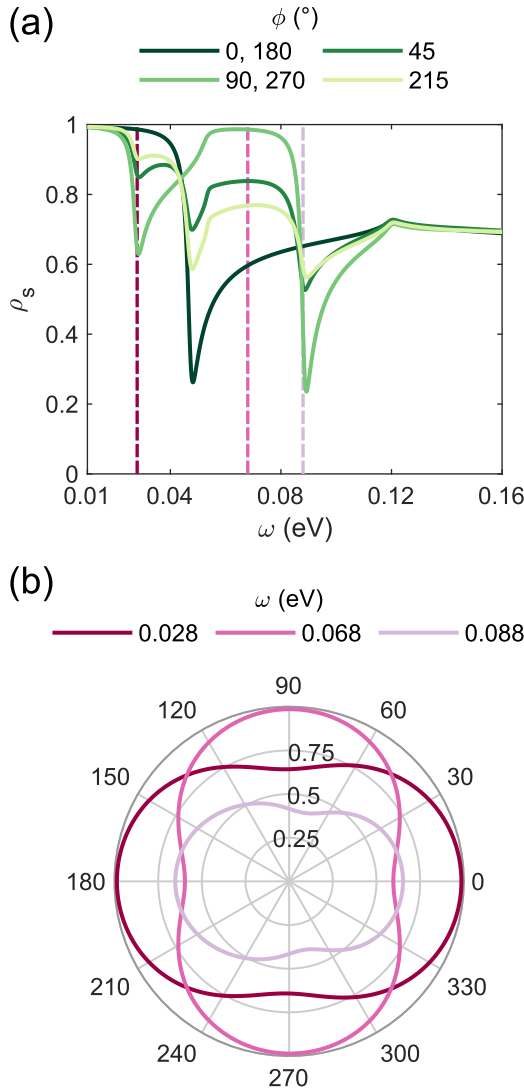


FIG. 4. (a) Reflectivity of s -polarized waves ρ_s as a function of the frequency ω and azimuthal angle of incidence ϕ at a polar angle of incidence $\theta = 60^\circ$ for $\phi = 0^\circ, 45^\circ, 90^\circ$, and 215° , with $\phi = 180^\circ$ and 270° being identical to $\phi = 0^\circ$ and 90° , respectively. (b) Polar plots of ρ_s at $\theta = 60^\circ$ and the frequencies 0.028, 0.068, and 0.088 eV, as indicated by the purple dotted lines in (a).

cases ($\phi = 45^\circ$ and 215°), the WSM supports two elliptically polarized waves, so both s - and p -polarized waves can couple to SPs. However, the wave vector has components normal and parallel to \mathbf{b} , meaning the SPs should be weakly nonreciprocal compared to the Voigt configuration and become reciprocal as the wave vector becomes parallel to \mathbf{b} . This is illustrated by Fig. 4(b), which shows polar plots of ρ_s at the frequencies highlighted by the dotted lines in Fig. 4(a), which include the reflectivity falling edges from Fig. 3(a) and 0.068 eV, a nonreciprocal frequency between 0.028 and 0.088 eV. The nonreciprocity is weak in the sense that the polar plots are only slightly asymmetric with respect to the y axis ($\phi = 90^\circ$).

B. Reflectivity of unpolarized light

To illustrate the overall nonreciprocity of the WSM, we calculated the reflectivity of unpolarized light,

given by

$$\rho(\omega, \theta, \phi) = \frac{\rho_p(\omega, \theta, \phi) + \rho_s(\omega, \theta, \phi)}{2}, \quad (4)$$

which we derive in Appendix C based on the randomness of unpolarized light emitted by thermal sources. Figure 5(a) shows polar plots of ρ at the approximate reflectivity falling edges, 0.028 and 0.088 eV, and $\theta = 60^\circ$. Clearly, ρ is nonreciprocal in the Voigt configuration ($\phi = 0^\circ$ and 180°) and reciprocal in the Faraday configuration ($\phi = 90^\circ$ and 270°). In between, the system appears to smoothly transition between the limiting cases as \mathbf{v}_{AHE} becomes normal to \mathbf{q} . Additionally, the polar plots in Fig. 5(a) appear very asymmetric compared to Fig. 4(b), suggesting that p -polarized waves dominate the nonreciprocity compared to s -polarized waves, which parallels our physical arguments and the general trends seen so far.

We also computed the difference in ρ at ϕ to ρ at $\phi + 180^\circ$ [15,40], equivalent to the difference between ϵ and α according to Eq. (1). Figure 5(b) shows plots of $\epsilon - \alpha$ as a function of ω and θ at $\phi = 0^\circ$. We observe the inequality between ϵ and α and thus the violation of Kirchhoff's law. Although $\epsilon - \alpha$ is largest near the reflectivity falling edges at $\theta = 60^\circ$, at $\theta = 89.3^\circ$, which we found maximizes $\epsilon - \alpha$, it is largest in between the reflectivity falling edges, specifically where the damped SP dispersion intersects the light line in between the “buckled” parts of the curve in Fig. 5(c), approximately 0.0545 and 0.0512 eV in the $\phi = 0^\circ$ and 180° directions, respectively. The maximum value of $\epsilon - \alpha$, approximately 0.40, is between these frequencies. Moreover, the nonreciprocity near 0.028 and 0.088 eV at $\theta = 89.3^\circ$ is small ($\epsilon - \alpha < 10^{-2}$), suggesting that at grazing incidence, incident waves no longer excite these modes. Physically, the longitudinal component of the electric field (the x component) vanishes at grazing incidence, meaning incident waves cannot excite the longitudinal SPs supported in the Voigt configuration such as those near the reflectivity falling edges in Fig. 3(a). However, they can still excite transverse SPs. The transverse component of the electric field of SPs (the z component, E_z) becomes much larger than the longitudinal component (the x component, E_x) in between the buckled parts of the damped SP dispersions, as shown in Fig. 5(c). In fact, $|E_z|/|E_x|$ peaks (or approaches $+\infty$ for undamped SPs) near the frequencies where $\epsilon - \alpha$ is the largest. Here, the nonreciprocity can be even larger than that of longitudinal SPs because \mathbf{v}_{AHE} is parallel to \mathbf{q} , meaning longitudinal retardation or acceleration due to the AHE is maximized [cf. Fig. 3(c)].

IV. CONCLUSION

This work demonstrated the violation of Kirchhoff's law on a flat WSM surface without an external magnetic field or grating structures. We showed that this violation of Kirchhoff's law is linked to nonreciprocal SPs supported by the WSM and that their nonreciprocity is caused by the Berry curvature-induced anomalous Hall effect. We believe that our results suggest a simple way to experimentally demonstrate the violation of Kirchhoff's law without an external magnetic field and could lead to the development of highly efficient

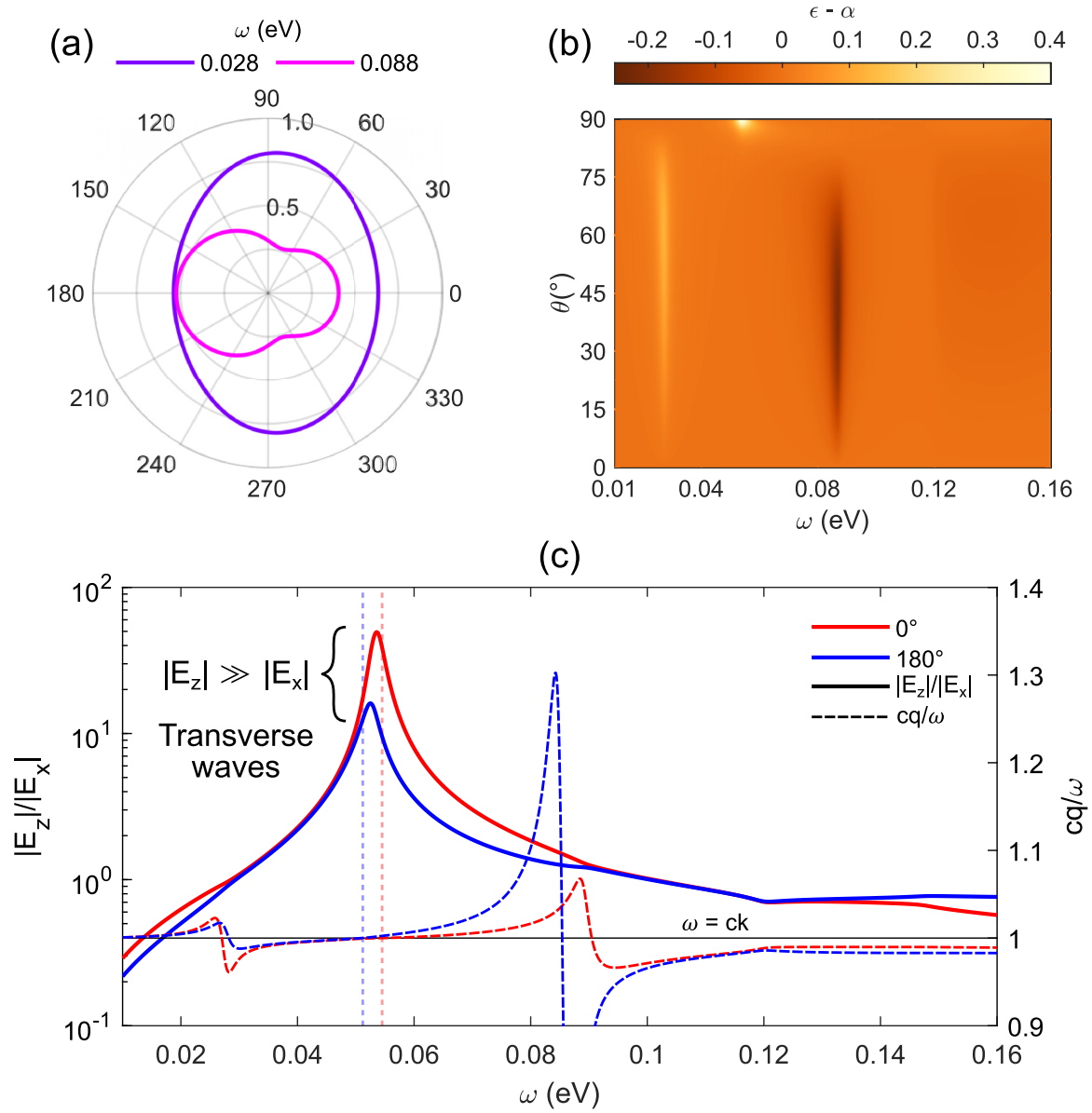


FIG. 5. (a) Polar plots of the reflectivity of unpolarized light ρ at polar angle of incidence $\theta = 60^\circ$ and the frequencies $\omega = 0.028$ and 0.088 eV. (b) Difference between the emissivity and absorptivity, $\epsilon - \alpha$, as a function of ω and θ at $\phi = 0^\circ$. (c) (Left axis) Ratio of the magnitude of the z component to the magnitude of the x component of the electric field of damped surface polaritons (SPs) $|E_z|/|E_x|$ at $\phi = 0^\circ$ and 180° . (Right axis) Real part of the damped surface polariton dispersion at $\phi = 0^\circ$ and 180° , reproduced from Fig. 3(d). The light red and light blue dotted lines indicate the frequencies at which the damped SP dispersions cross the light line, $\omega = ck$, in between the buckled parts of the curves. The SPs are transverse waves at these frequencies, as indicated.

photovoltaic and thermophotovoltaic cells as well as smaller, simpler nonreciprocal optical instruments.

ACKNOWLEDGMENTS

This work is supported by ARO MURI (Grant No. W911NF-19-1-0279) via the University of Michigan. The authors acknowledge computational support from the Stampede2 supercomputer and the Extreme Science and Engineering Discovery Environment (XSEDE).

APPENDIX A: DETAILS OF THE REFLECTIVITY CALCULATION

1. General equations

In this work, we used the exact 2×2 reflection matrix method developed by Abdulhalim [33] to compute the reflectivity. Here, we outline the method and provide the analytical expressions for the dispersion relation and the eigenvectors from which the electric and magnetic field matrices E_{ijl} and H_{ijl} used in Eq. (4) were computed.

By decomposing Maxwell's equations in an arbitrary, non-magnetic medium and assuming plane-wave solutions, it is

$$\begin{bmatrix} -s_x s_y - \varepsilon_{yx} - b_x (s_y s_z + \varepsilon_{yz}) & s_x^2 + s_z^2 - \varepsilon_{yy} - b_y (s_y s_z + \varepsilon_{yz}) \\ -s_y^2 - s_z^2 + \varepsilon_{xx} + b_x (s_x s_z + \varepsilon_{xz}) & s_x s_y + \varepsilon_{xy} + b_y (s_x s_y + \varepsilon_{zz}) \end{bmatrix} \Psi_e = 0, \quad (\text{A1})$$

where ε_{ij} are the components of the dielectric tensor ($i, j = x, y, z$), $b_x = (\varepsilon_{zx} + s_x s_z) / (s_x^2 + s_y^2 - \varepsilon_{zz})$, $b_y = (\varepsilon_{zy} + s_y s_z) / (s_x^2 + s_y^2 - \varepsilon_{zz})$, and $\Psi_e = \sqrt{\varepsilon_0} e^{i(\omega/c) s_z z} [E_x \ E_y]^T$. Likewise, it can be shown that $\Psi_h = \sqrt{\mu_0} e^{i(\omega/c) s_z z} [H_x \ H_y]^T$ is related to Ψ_e by

$$\Psi_h = \begin{bmatrix} b_x s_y & b_y s_y - s_z \\ -b_x s_x + s_z & -b_y s_x \end{bmatrix} \Psi_e. \quad (\text{A2})$$

It is easy to see that in the coordinate system defined in Fig. 1, Ψ_e and Ψ_h are essentially the tangential components of the electric and magnetic fields, respectively.

Equation (A1) has nontrivial solutions if and only if the determinant of the matrix on the left-hand side (called G) is zero (i.e., $|G| = 0$). This can be used to solve for s_z , which is unknown, and equivalently, the dispersion relation, which has the form

$$s_z^4 + a s_z^3 + b s_z^2 + c s_z + d = 0 \quad (\text{A3})$$

in general. In air, Eq. (A3) takes on the more familiar form $s_z = \sqrt{1 - s_x^2 - s_y^2}$, and in WSMs, it can be shown that $a = c = 0$ (under any rotation in the xy plane), leading to the explicit solution

$$s_z = \pm \sqrt{\frac{-b \pm \sqrt{b^2 - 4d}}{2}}. \quad (\text{A4})$$

For WSMs, this is also the bulk plasmon dispersion. Equations (A11) and (A12), to be presented later, give b and d . Equation (A4) shows that there are four propagation modes in WSMs: two forward ($s_z > 0$), which we denote 1 and 2, and two backward ($s_z < 0$), 3 and 4. (Technically, there are four propagation modes in air as well, but the wave vectors of modes 1 and 2 and modes 3 and 4, respectively, are degenerate.) Once s_z is known, so are the electric- and magnetic-field vectors by Eqs. (A1) and (A2).

The reflection matrix in the (x, y) basis, R_{xy} , can be found by applying the solutions to Eqs. (A1) and (A2) to the standard electromagnetic interface conditions: continuity of the tangential component of the electric field,

$$\Psi_e|_{z=0^+} = \Psi_e|_{z=0^-}, \quad (\text{A5})$$

and continuity of the tangential component of the magnetic field,

$$\Psi_h|_{z=0^+} = \Psi_h|_{z=0^-}. \quad (\text{A6})$$

Equations (A5) and (A6) do not account for the effects of Fermi arc surface states, although their inclusion is relatively straightforward following Ref. [21] and transform the homogeneous boundary conditions into inhomogeneous ones. From Eqs. (A5) and (A6), it is possible to obtain

$$R_{xy} = (E_{12n}^{-1} E_{34m} - H_{12n}^{-1} H_{34m})^{-1} (H_{12n}^{-1} H_{12m} - E_{12n}^{-1} E_{12m}),$$

possible to show that the x - and y components of the electric field vector are governed by the homogeneous system

$$(\text{A7})$$

where $E_{ijl} = (V_{ei} U_{ej})_l$ and $H_{ijl} = (V_{hi} U_{hj})_l$; $i, j = 1, 2, 3, 4$ denote propagation modes, $l = m, n$ denote the lower ($m, z < 0$) or upper ($n, z > 0$) medium, and V_e and U_e are the eigenvectors of Eq. (A1), with V_h and U_h found by substituting V_e and U_e into Eq. (A2). If m is air, it can be shown that $E_{12m} = E_{34m} = \mathbb{I}$, where \mathbb{I} is the identity matrix, and $H_{12m} = -H_{34m}$. This simplifies Eq. (A7) to

$$R_{xy} = (E_{12n}^{-1} + H_{12n}^{-1} H_{12m})^{-1} (H_{12n}^{-1} H_{12m} - E_{12n}^{-1}). \quad (\text{A8})$$

R_{xy} can be transformed into the (p, s) basis (i.e., p - and s -polarizations) using the transformation matrix

$$T = \begin{bmatrix} \frac{s_{z1,2m} s_x}{s_{xy}} & -\frac{s_y}{s_{xy}} \\ \frac{s_{z1,2m} s_y}{s_{xy}} & \frac{s_x}{s_{xy}} \end{bmatrix}, \quad (\text{A9})$$

where $s_{z1,2m}$ is the z component of the wave vector of the forward-propagating modes in air and $s_{xy} = \sqrt{s_x^2 + s_y^2}$ is the in-plane wave vector. Then

$$\begin{bmatrix} r_{p,p} & r_{p,s} \\ r_{s,p} & r_{s,s} \end{bmatrix} = T^{-1} R_{xy} T. \quad (\text{A10})$$

Thus, the reflectivity of p - and s -polarized waves are $\rho_p = |r_{p,p}|^2 + |r_{p,s}|^2$ and $\rho_s = |r_{s,s}|^2 + |r_{s,p}|^2$, accounting for mode conversion via the $r_{p,s}$ and $r_{s,p}$ (i.e., conversion of an incident p -polarized wave to a reflected s -polarized wave and vice versa). The coefficients of Eq. (A4) are

$$b = \frac{1}{\varepsilon_{zz}} (s_x^2 (\varepsilon_{xx} + \varepsilon_{zz}) + s_y^2 (\varepsilon_{yy} + \varepsilon_{zz}) + (g^2 - (\varepsilon_{xx} + \varepsilon_{yy}) \varepsilon_{zz})), \quad (\text{A11})$$

$$d = \frac{1}{\varepsilon_{zz}} (s_x^4 \varepsilon_{xx} + s_x^2 (g^2 + s_y^2 (\varepsilon_{xx} + \varepsilon_{yy}) - \varepsilon_{xx} (\varepsilon_{yy} + \varepsilon_{zz})) - \varepsilon_{yy} (g^2 - (s_y^2 - \varepsilon_{xx}) (s_y^2 - \varepsilon_{zz}))). \quad (\text{A12})$$

The eigenvectors are

$$V_{ej} = \frac{1}{\sqrt{1 + \xi_j \xi_j^*}} \begin{bmatrix} 1 \\ \xi_j \end{bmatrix}, \quad (\text{A13})$$

$$U_{ej} = \frac{1}{\sqrt{1 + \chi_j \chi_j^*}} \begin{bmatrix} \chi_j \\ 1 \end{bmatrix}. \quad (\text{A14})$$

The subscript j denotes the mode of propagation ($j = 1, 2, 3, 4$). The expressions for the coefficients ξ_j and χ_j

(also known as the polarization ratios [33]) are

$$\xi_j = \frac{s_y^4 + s_x^2(s_y^2 - \varepsilon_{xx}) + s_y^2(s_{zj}^2 - \varepsilon_{xx} - \varepsilon_{zz}) - g^2 - (s_{zj}^2 - \varepsilon_{xx})\varepsilon_{zz}}{s_x^3 s_y + s_x s_y^3 + s_x s_y (s_{zj}^2 - \varepsilon_{zz}) + s_y s_{zj} \varepsilon_{zz}}, \quad (\text{A15})$$

$$\chi_j = \frac{s_x^2 + s_{zj}^2 (1 - s_y^2 / (s_x^2 + s_y^2 - \varepsilon_{zz})) - \varepsilon_{yy}}{s_x s_y + s_y s_{zj} (-ig + s_x s_{zj}) / (s_x^2 + s_y^2 - \varepsilon_{zz})}. \quad (\text{A16})$$

Lastly, to compute the magnetic-field eigenvectors V_{hj} and U_{hj} , we used Eq. (A2) (i.e., $V_{hj} = Q_j V_{ej}$ and $U_{hj} = Q_j U_{ej}$), where

$$Q_j = \begin{bmatrix} \frac{s_y(-ig+s_x s_{zj})}{s_x^2+s_y^2-\varepsilon_{zz}} & s_{zj} \left(\frac{s_y^2}{s_x^2+s_y^2-\varepsilon_{zz}} - 1 \right) \\ s_{zj} - \frac{s_x(-ig+s_x s_{zj})}{s_x^2+s_y^2-\varepsilon_{zz}} & -\frac{s_x s_y s_{zj}}{s_x^2+s_y^2-\varepsilon_{zz}} \end{bmatrix}. \quad (\text{A17})$$

2. Voigt configuration

In the Voigt configuration, it is possible to get simple expressions for the bulk plasmon dispersion and the reflectivity. In Eq. (A4), assuming s_z is positive, there are two possible bulk plasmon modes: the ordinary mode O with $s_{z1} = \sqrt{(-b + \sqrt{b^2 - 4d})/2}$ and the extraordinary mode X with $s_{z2} = \sqrt{(-b - \sqrt{b^2 - 4d})/2}$, where 1 and 2 are used to respect the notation in the previous section. Using these, the ordinary and extraordinary effective indices of refraction can be defined as $n_O = \sqrt{s_x^2 + s_y^2 + s_{z1}^2}$ and $n_X = \sqrt{s_x^2 + s_y^2 + s_{z2}^2}$. For propagation in the positive x direction, $\phi = 0^\circ$, $s_x = \sin \theta$, and $s_y = 0$. In this case, it can be shown that

$$s_{z1} = \sqrt{\varepsilon_{yy} - \sin^2 \theta}, \quad (\text{A18})$$

$$s_{z2} = \sqrt{\frac{-g^2 - \varepsilon_{xx}(\sin^2 \theta - \varepsilon_{zz})}{\varepsilon_{zz}}}. \quad (\text{A19})$$

Using Eqs. (A18) and (A19) and following the method described in the previous section, it is possible to derive the reflection coefficients in the Voigt configuration. It is important to recognize that in this direction, $s_y = 0$ and ξ , $\chi \rightarrow \infty$, meaning the electric-field eigenvectors are $V_{e1} = [0 \ 1]^T$ and $U_{e2} = [1 \ 0]^T$. Thus, it can be shown that in the $+x$ direction ($\phi = 0^\circ$),

$$r_{s,s} = \frac{\cos \theta - s_{z1}}{\cos \theta + s_{z1}}, \quad (\text{A20})$$

$$r_{p,p} = \frac{\varepsilon_{zz}(\sec \theta - s_{z2}) + \sin \theta(ig - \tan \theta)}{\varepsilon_{zz}(\sec \theta + s_{z2}) - \sin \theta(ig + \tan \theta)}, \quad (\text{A21})$$

$$r_{s,p} = r_{p,s} = 0. \quad (\text{A22})$$

In the $-x$ direction ($\phi = 180^\circ$),

$$r_{s,s} = \frac{\cos \theta - s_{z1}}{\cos \theta + s_{z1}}, \quad (\text{A23})$$

$$r_{p,p} = \frac{\varepsilon_{zz}(\sec \theta - s_{z2}) - \sin \theta(ig + \tan \theta)}{\varepsilon_{zz}(\sec \theta + s_{z2}) + \sin \theta(ig - \tan \theta)}, \quad (\text{A24})$$

$$r_{s,p} = r_{p,s} = 0. \quad (\text{A25})$$

Equations (A20) and (A23) are identical, showing that s -polarized waves are reciprocal in the Voigt configuration, while Eqs. (A21) and (A24) show that p -polarized waves are nonreciprocal.

APPENDIX B: DERIVATION OF THE SURFACE POLARITON DISPERSION

1. Voigt configuration

In the main text, we argued that the nonreciprocal reflectivity in the Voigt and Faraday configurations, respectively, are due to coupling to SPs, which are nonreciprocal in the former configuration but not in the latter. Here, we derive the dispersion relations of SPs in each configuration following Ref. [41] but in our notation for the sake of completeness.

Consider a semi-infinite WSM in the half space $z > 0$ with its \mathbf{b} vector pointing in the y direction. The other half space $z < 0$ is air (refractive index $n = 1$). We seek the dispersion relation of SPs propagating normal to the \mathbf{b} vector. In particular, we seek solutions of the electromagnetic wave equation in the WSM of the form

$$\mathbf{E}_1 = [1 \ 0 \ E_{z1}]^T \eta e^{-\alpha_1 z}, \quad (\text{B1})$$

where $\eta = e^{i\omega t - iqx}$. We can seek solutions of this form because we know that the WSM supports s - and p -polarized waves in this configuration, and only p -polarized waves are longitudinal. The corresponding electric field in air is

$$\mathbf{E}_0 = [1 \ 0 \ E_{z0}]^T \eta e^{\alpha_0 z}. \quad (\text{B2})$$

We can find the decay constants α_1 and α_0 using the electromagnetic wave equation. In particular, we can write it in the form $\hat{M}\mathbf{E} = 0$, where

$$\hat{M} = \begin{bmatrix} -k_y^2 - k_z^2 & k_x k_y & k_x k_z \\ k_x k_y & -k_x^2 - k_z^2 & k_y k_z \\ k_x k_z & k_y k_z & -k_x^2 - k_y^2 \end{bmatrix} + k_0^2 \bar{\varepsilon}(\omega). \quad (\text{B3})$$

Here, $k_0 = \omega/c$ is the magnitude of the wave vector in vacuum and $\bar{\varepsilon}(\omega)$ is the dielectric tensor. Equation (B3) has nontrivial solutions if and only if $|\hat{M}| = 0$, from which we can derive the equations for the decay constants. In air, it can be shown that

$$\alpha_0 = \sqrt{q^2 - k_0^2}. \quad (\text{B4})$$

In the WSM, the decay constant is

$$\alpha_1 = \sqrt{\frac{\varepsilon_{xx} q^2}{\varepsilon_{zz}} - \frac{(\varepsilon_{xx} \varepsilon_{zz} - g^2) k_0^2}{\varepsilon_{zz}}}. \quad (\text{B5})$$

We can make a few observations about the electric and magnetic fields. First, using the electromagnetic wave equation, we can determine E_{z0} and E_{z1} :

$$\begin{bmatrix} k_0^2 + \alpha_0^2 & 0 & i\alpha_0 q \\ 0 & k_0^2 - q^2 + \alpha_0^2 & 0 \\ i\alpha_0 q & 0 & k_0^2 - q^2 \end{bmatrix} \begin{bmatrix} 1 \\ 0 \\ E_{z0} \end{bmatrix} = 0 \Rightarrow E_{z0} = iq/\alpha_0, \quad (\text{B6})$$

$$\begin{bmatrix} k_0^2 \varepsilon_{xx} + \alpha_1^2 & 0 & -i\alpha_1 q + igk_0^2 \\ 0 & k_0^2 \varepsilon_{yy} - q^2 + \alpha_1^2 & 0 \\ -i\alpha_1 q - igk_0^2 & 0 & k_0^2 \varepsilon_{zz} - q^2 \end{bmatrix} \begin{bmatrix} 1 \\ 0 \\ E_{z1} \end{bmatrix} = 0 \Rightarrow E_{z1} = \frac{i(\alpha_1 q + gk_0^2)}{k_0^2 \varepsilon_{zz} - q^2}. \quad (\text{B7})$$

We can also determine the magnetic-field vectors using Faraday's law:

$$\nabla \times \mathbf{E} = -\frac{\partial \mathbf{B}}{\partial t}. \quad (\text{B8})$$

In air,

$$\mathbf{B}_0 = \omega^{-1} [0 \quad -qE_{z0} + i\alpha_0 \quad 0]^T \eta e^{\alpha_0 z}, \quad (\text{B9})$$

and in the WSM,

$$\mathbf{B}_1 = -\omega^{-1} [0 \quad qE_{z1} + i\alpha_1 \quad 0]^T \eta e^{-\alpha_1 z}. \quad (\text{B10})$$

To obtain the dispersion relation for the in-plane wave vector q , we apply the standard electromagnetic boundary conditions at $z = 0$. Namely, these are continuity of D_z ,

$$E_{z0} = -ig + \varepsilon_{zz} E_{z1}, \quad (\text{B11})$$

and continuity of B_y ,

$$-qE_{z0} + i\alpha_0 = -qE_{z1} - i\alpha_1. \quad (\text{B12})$$

In reality, only three equations out of Eqs. (B6) and (B7) and Eqs. (B11) and (B12) are needed to solve for q . For example, we can substitute Eq. (B6) into Eqs. (B11) and (B12):

$$\frac{iq}{\alpha_0} = -ig + \varepsilon_{zz} E_{z1} \Rightarrow E_{z1} = \frac{i(q + g\alpha_0)}{\varepsilon_{zz} \alpha_0},$$

$$-q \left(\frac{iq}{\alpha_0} \right) + i\alpha_0 = -qE_{z1} - i\alpha_1$$

$$\Rightarrow E_{z1} = \frac{i(q^2 - \alpha_0^2 - \alpha_0 \alpha_1)}{q\alpha_0}.$$

Setting the resulting expressions equal to each other and writing the equation in terms of q , we obtain the SP dispersion in the Voigt configuration:

$$q^2 + g\alpha_0 q + \varepsilon_{zz}(\alpha_0 \alpha_1 - k_0^2) = 0. \quad (\text{B13})$$

Using MATHEMATICA (version 12.0.0.0), we found the exact solutions of Eq. (B13):

$$q = \pm \sqrt{\frac{g^4 - g^2 \pm \mathcal{A} + \mathcal{B}}{(g^2 - 1)^2 - 2(g^2 + 1)\varepsilon_{xx}\varepsilon_{zz} + (\varepsilon_{xx}\varepsilon_{zz})^2}}, \quad (\text{B14})$$

where

$$\mathcal{A} = 2g\sqrt{\varepsilon_{zz}(g^2 + \varepsilon_{xx} + \varepsilon_{zz} - \varepsilon_{xx}\varepsilon_{zz} - 1)}, \quad (\text{B15})$$

$$\mathcal{B} = \varepsilon_{zz}(g^2 + 1 + \varepsilon_{xx}[\varepsilon_{zz}(\varepsilon_{xx} - 1) - 1 - 2g^2]). \quad (\text{B16})$$

Near the resonance frequencies, the undamped SPs can merge with the bulk plasmons, whose dispersion can be found by letting $\alpha_1 = 0$ and solving for q in Eq. (B3):

$$q = k_0 \sqrt{\varepsilon_{zz} - g^2/\varepsilon_{xx}}. \quad (\text{B17})$$

2. Faraday configuration

Continuing from the previous section, now we seek solutions of the form

$$\mathbf{E} = t_1 \mathbf{E}_1 + t_2 \mathbf{E}_2,$$

$$\mathbf{E}_1 = [E_{x1} \quad 1 \quad E_{z1}]^T \eta e^{-\alpha_1 z}, \quad (\text{B18})$$

$$\mathbf{E}_2 = [E_{x2} \quad 1 \quad E_{z2}]^T \eta e^{-\alpha_2 z}. \quad (\text{B19})$$

This is because the bulk WSM supports two elliptically polarized waves. Thus, we cannot assume that the surface waves are strictly s - and p polarized, and the total surface wave is the superposition of the two surface waves supported by the WSM. The electric field in air is

$$\mathbf{E}_0 = [E_{x0} \quad 1 \quad E_{z0}]^T \eta e^{\alpha_0 z}. \quad (\text{B20})$$

Once again, we can find the decay constants using the determinant of Eq. (B3). The decay constant in air is still given by Eq. (B4). In the WSM, we have two decay constants:

$$\alpha_m = \sqrt{\frac{\mathcal{C} \pm \sqrt{\mathcal{D}}}{2\varepsilon_{zz}}}, \quad (\text{B21})$$

where $m = 1, 2$ and

$$\mathcal{C} = q^2(\varepsilon_{yy} + \varepsilon_{zz}) + k_0^2(g^2 - (\varepsilon_{xx} + \varepsilon_{yy})\varepsilon_{zz}), \quad (\text{B22})$$

$$\mathcal{D} = (g^2 k_0^2 + \varepsilon_{yy} q^2)^2 + 2(g^2 k_0^2 - \varepsilon_{yy} q^2)(q^2 + k_0^2(-\varepsilon_{xx} + \varepsilon_{yy}))\varepsilon_{zz} + (q^2 + k_0^2(-\varepsilon_{xx} + \varepsilon_{yy}))^2 \varepsilon_{zz}^2. \quad (\text{B23})$$

Like before, we can determine the electric fields:

$$\begin{bmatrix} k_0^2 - q^2 + \alpha_0^2 & 0 & 0 \\ 0 & k_0^2 + \alpha_0^2 & i\alpha_0 q \\ 0 & i\alpha_0 q & k_0^2 - q^2 \end{bmatrix} \begin{bmatrix} E_{x0} \\ 1 \\ E_{z0} \end{bmatrix} = 0 \Rightarrow E_{z0} = iq/\alpha_0, \quad (\text{B24})$$

$$\begin{bmatrix} k_0^2 \varepsilon_{xx} - q^2 + \alpha_m^2 & 0 & igk_0^2 \\ 0 & k_0^2 \varepsilon_{yy} + \alpha_m^2 & -i\alpha_m q \\ -igk_0^2 & -i\alpha_m q & k_0^2 \varepsilon_{zz} - q^2 \end{bmatrix} \begin{bmatrix} E_{xm} \\ 1 \\ E_{zm} \end{bmatrix} = 0 \Rightarrow E_{zm} = -\frac{i(k_0^2 \varepsilon_{yy} + \alpha_m^2)}{\alpha_m q}, \quad (\text{B25})$$

$$E_{xm} = -\frac{igk_0^2}{k_0^2\varepsilon_{xx} - q^2 + \alpha_m^2}E_{zm} = -\frac{gk_0^2(k_0^2\varepsilon_{yy} + \alpha_m^2)}{\alpha_m q(k_0^2\varepsilon_{xx} - q^2 + \alpha_m^2)}. \quad (\text{B26})$$

We can also determine the magnetic fields using Eq. (B8):

$$\mathbf{B}_m = \omega^{-1}[i\alpha_m + qE_{zm} \quad -i\alpha_mE_{xm} \quad -qE_{xm}]^T \eta e^{-\alpha_m z}, \quad (\text{B27})$$

$$\mathbf{B}_0 = \omega^{-1}[-i\alpha_0 + qE_{z0} \quad i\alpha_0 E_{x0} \quad -qE_{x0}]^T \eta e^{\alpha_0 z}. \quad (\text{B28})$$

Once again, we apply the standard electromagnetic boundary conditions at $z = 0$ to determine q . In this case, we need more boundary conditions because we have more unknowns than before. First, we have continuity of E_x :

$$E_{x0} = t_1 E_{x1} + t_2 E_{x2}. \quad (\text{B29})$$

Second, we have continuity of B_y :

$$\alpha_0 E_{x0} = -t_1 \alpha_1 E_{x1} - t_2 \alpha_2 E_{x2}. \quad (\text{B30})$$

Multiplying Eq. (B29) by α_0 and subtracting it from Eq. (B30) gives us

$$t_2 = -\frac{(\alpha_0 + \alpha_1)E_{x1}}{(\alpha_0 + \alpha_2)E_{x2}} t_1. \quad (\text{B31})$$

Then, continuity of E_y gives us

$$1 = t_1 + t_2. \quad (\text{B32})$$

Rearranging Eq. (B32) and substituting it into Eq. (B31), we find that

$$t_1 = \frac{(\alpha_0 + \alpha_2)E_{x2}}{(\alpha_0 + \alpha_2)E_{x2} - (\alpha_0 + \alpha_1)E_{x1}}, \quad (\text{B33})$$

$$t_2 = \frac{(\alpha_0 + \alpha_1)E_{x1}}{(\alpha_0 + \alpha_1)E_{x1} - (\alpha_0 + \alpha_2)E_{x2}}. \quad (\text{B34})$$

Lastly, we have continuity of B_x :

$$-i\alpha_0 + qE_{z0} = t_1(i\alpha_1 + qE_{z1}) + t_2(i\alpha_2 + qE_{z2}). \quad (\text{B35})$$

Everything in Eq. (B35) can be written in terms of q and the known variables. This allows us to solve for the dispersion relation in the Faraday configuration (although the algebra is rather tedious):

$$0 = (\alpha_0\varepsilon_{yy} + \alpha_2)(q^2 - k_0^2\varepsilon_{xx} - \alpha_2^2)(\alpha_0 + \alpha_1)(k_0^2\varepsilon_{yy} + \alpha_1^2) - (\alpha_0\varepsilon_{yy} + \alpha_1)(q^2 - k_0^2\varepsilon_{xx} - \alpha_1^2)(\alpha_0 + \alpha_2)(k_0^2\varepsilon_{yy} + \alpha_2^2). \quad (\text{B36})$$

The dispersion of the bulk plasmons with which the SPs can merge is given by

$$q = \frac{k_0}{\sqrt{2}} \sqrt{\varepsilon_{xx} + \varepsilon_{zz} \pm \sqrt{(\varepsilon_{xx} - \varepsilon_{zz})^2 - 4g^2}}. \quad (\text{B37})$$

APPENDIX C: DERIVATION OF THE REFLECTIVITY OF UNPOLARIZED LIGHT

Consider a generally polarized incident wave reflecting off of a general anisotropic medium ($z > 0$) in the xz plane (without loss of generality). Letting s be the fraction of the intensity s -polarized light in the incident wave and φ be the phase difference between the s - and p -polarized components, we can write the electric and magnetic fields of the incident wave:

$$\mathbf{E}_i = E_i[\sqrt{1-s}\cos\theta \quad \sqrt{s}e^{i\varphi} \quad -\sqrt{1-s}\sin\theta]^T \times e^{i(\omega t - \mathbf{k}_i \cdot \mathbf{r})}, \quad (\text{C1})$$

$$\mathbf{H}_i = Z_0^{-1}E_i[-\sqrt{s}e^{i\varphi}\cos\theta \quad \sqrt{1-s} \quad \sqrt{s}e^{i\varphi}\sin\theta]^T \times e^{i(\omega t - \mathbf{k}_i \cdot \mathbf{r})}, \quad (\text{C2})$$

where $\mathbf{k}_i = (\omega/c)[\sin\theta \quad 0 \quad \cos\theta]^T$ and $Z_0 = \sqrt{\mu_0/\varepsilon_0}$ is the impedance of free space. Similarly, for the reflected wave, we can write:

$$\mathbf{E}_r = [E_{r,p}\cos\theta \quad E_{r,s} \quad E_{r,p}\sin\theta]^T e^{i(\omega t - \mathbf{k}_r \cdot \mathbf{r})}, \quad (\text{C3})$$

$$\mathbf{H}_r = Z_0^{-1}[E_{r,s}\cos\theta \quad -E_{r,p} \quad E_{r,s}\sin\theta]^T e^{i(\omega t - \mathbf{k}_r \cdot \mathbf{r})}, \quad (\text{C4})$$

where $\mathbf{k}_r = (\omega/c)[\sin\theta \quad 0 \quad -\cos\theta]^T$. The reflectivity is defined as

$$R = -\frac{\langle S_{z,r} \rangle}{\langle S_{z,i} \rangle}, \quad (\text{C5})$$

where $\langle S_{z,i} \rangle$ and $\langle S_{z,r} \rangle$ are the z components of the time-averaged Poynting vectors of the incident and reflected waves, respectively:

$$\langle S_z \rangle = \frac{1}{2} \text{Re}(\hat{\mathbf{z}} \cdot \mathbf{E} \times \mathbf{H}^*). \quad (\text{C6})$$

The negative sign in Eq. (C5) accounts for the direction of $\langle S_{z,r} \rangle$ (energy exiting the system). By carrying out the cross product in Eq. (C6), it can be shown that

$$\langle S_{z,i} \rangle = \frac{\cos\theta}{2Z_0} |E_i|^2, \quad (\text{C7})$$

$$\langle S_{z,r} \rangle = -\frac{\cos\theta}{2Z_0} (|E_{r,p}|^2 + |E_{r,s}|^2), \quad (\text{C8})$$

and hence

$$R = \frac{|E_{r,p}|^2 + |E_{r,s}|^2}{|E_i|^2}. \quad (\text{C9})$$

Now we use the fact that $E_{r,p} = r_{p,p}\sqrt{1-s}E_i + r_{s,p}\sqrt{s}E_i e^{i\varphi}$ and $E_{r,s} = r_{s,s}\sqrt{s}E_i e^{i\varphi} + r_{p,s}\sqrt{1-s}E_i$ to write Eq. (C9) in terms of the reflection coefficients. Substituting these expressions into Eq. (C9) and simplifying, we find that

$$R = (1-s)\rho_p + s\rho_s + 2\sqrt{s}\sqrt{1-s} \times \text{Re}[(r_{p,p}r_{s,p}^* + r_{s,s}^*r_{p,s})e^{-i\varphi}], \quad (\text{C10})$$

where ρ_p and ρ_s are defined as before. Equation (C10) is the reflectivity of an incident wave with a general polarization defined as a composition of s - and p -polarized waves, parametrized by $0 \leq s \leq 1$ and $0 \leq \varphi < 2\pi$. This equation suggests that for light that is not purely s - or p polarized, the reflectivity consists of a weighted average of the s - and p -polarized reflectivities (the first two terms) and an interfer-

ence term. This interference term accounts for the interference between reflected waves of the same polarization produced by incident waves with different polarizations. The reflectivity of unpolarized light is simply Eq. (C10) averaged over all possible polarizations:

$$\rho = \frac{1}{2\pi} \int_0^1 \int_0^{2\pi} R d\varphi ds \Rightarrow \rho = \frac{\rho_s + \rho_p}{2}. \quad (\text{C11})$$

-
- [1] G. Kirchhoff, *Ann. Phys. Chem.* **185**, 275 (1860).
- [2] J. R. Howell, M. P. Mengüç, and R. Siegel, *Thermal Radiation Heat Transfer*, 6th ed. (CRC Press, Boca Raton, FL, 2016).
- [3] W. C. Snyder, Z. Wan, and X. Li, *Appl. Opt.* **37**, 3464 (1998).
- [4] L. Zhu and S. Fan, *Phys. Rev. B* **90**, 220301(R) (2014).
- [5] Y. Tsurimaki, X. Qian, S. Pajovic, F. Han, M. Li, and G. Chen, *Phys. Rev. B* **101**, 165426 (2020).
- [6] B. Hapke, *Theory of Reflectance and Emittance Spectroscopy*, 2nd ed. (Cambridge University Press, New York, 2012).
- [7] L. Remer, E. Mohler, W. Grill, and B. Lüthi, *Phys. Rev. B* **30**, 3277 (1984).
- [8] M. A. Green, *Nano Lett.* **12**, 5985 (2012).
- [9] H. Ries, *Appl. Phys. B: Photophys. Laser Chem.* **32**, 153 (1983).
- [10] J. Yu, H. Chen, Y. Wu, and S. Liu, *EPL (Europhysics Lett.)* **100**, 47007 (2012).
- [11] V. S. Asadchy, C. Guo, B. Zhao, and S. Fan, *Adv. Opt. Mater.* **8**, 2000100 (2020).
- [12] A. K. Zvezdin and V. A. Kotov, *Modern Magneto-optics and Magneto-optical Materials*, 1st ed. (Taylor & Francis Group, New York, 1997).
- [13] L. D. Landau and E. M. Lifshitz, *Electrodynamics of Continuous Media*, 2nd ed. (Pergamon Press Ltd., Elmsford, NY, 1984).
- [14] F. L. Pedrotti, L. M. Pedrotti, and L. S. Pedrotti, *Introduction to Optics*, 3rd ed. (Cambridge University Press, Cambridge, UK, 2018).
- [15] B. Zhao, C. Guo, C. A. C. Garcia, P. Narang, and S. Fan, *Nano Lett.* **20**, 1923 (2020).
- [16] B. Zhao, Y. Shi, J. Wang, Z. Zhao, N. Zhao, and S. Fan, *Opt. Lett.* **44**, 4203 (2019).
- [17] N. Nagaosa, J. Sinova, S. Onoda, A. H. MacDonald, and N. P. Ong, *Rev. Mod. Phys.* **82**, 1539 (2010).
- [18] N. Morali, R. Batabyal, P. K. Nag, E. Liu, Q. Xu, Y. Sun, B. Yan, C. Felser, N. Avraham, and H. Beidenkopf, *Science* **365**, 1286 (2019).
- [19] E. Liu, Y. Sun, N. Kumar, L. Muechler, A. Sun, L. Jiao, S.-Y. Yang, D. Liu, A. Liang, Q. Xu, J. Kroder, V. Süß, H. Borrmann, C. Shekhar, Z. Wang, C. Xi, W. Wang, W. Schnelle, S. Wirth, Y. Chen, S. T. B. Goennenwein, and C. Felser, *Nat. Phys.* **14**, 1125 (2018).
- [20] B. Yan and C. Felser, *Annu. Rev. Condens. Matter Phys.* **8**, 337 (2017).
- [21] Q. Chen, A. R. Kutayiah, I. Oladyskhin, M. Tokman, and A. Belyanin, *Phys. Rev. B* **99**, 075137 (2019).
- [22] Q. Chen, M. Erukhimova, M. Tokman, and A. Belyanin, *Phys. Rev. B* **100**, 235451 (2019).
- [23] O. V. Kotov and Y. E. Lozovik, *Phys. Rev. B* **98**, 195446 (2018).
- [24] A. A. Zyuzin and V. A. Zyuzin, *Phys. Rev. B* **92**, 115310 (2015).
- [25] M. Kargarian, M. Randeria, and N. Trivedi, *Sci. Rep.* **5**, 12683 (2015).
- [26] P. S. Pershan, *J. Appl. Phys.* **38**, 1482 (1967).
- [27] Q. Wang, Y. Xu, R. Lou, Z. Liu, M. Li, Y. Huang, D. Shen, H. Weng, S. Wang, and H. Lei, *Nat. Commun.* **9**, 3681 (2018).
- [28] K. Kuroda, T. Tomita, M.-T. Suzuki, C. Bareille, A. A. Nugroho, P. Goswami, M. Ochi, M. Ikhlas, M. Nakayama, S. Akebi, R. Noguchi, R. Ishii, N. Inami, K. Ono, H. Kumigashira, A. Varykhalov, T. Muro, T. Koretsune, R. Arita, S. Shin, T. Kondo, and S. Nakatsuji, *Nat. Mater.* **16**, 1090 (2017).
- [29] I. Belopolski, K. Manna, D. S. Sanchez, G. Chang, B. Ernst, J. Yin, S. S. Zhang, T. Cochran, N. Shumiya, H. Zheng, B. Singh, G. Bian, D. Multer, M. Litskevich, X. Zhou, S.-M. Huang, B. Wang, T.-R. Chang, S.-Y. Xu, A. Bansil, C. Felser, H. Lin, and M. Z. Hasan, *Science* **365**, 1278 (2019).
- [30] P. Hosur, S. A. Parameswaran, and A. Vishwanath, *Phys. Rev. Lett.* **108**, 046602 (2012).
- [31] A. B. Sushkov, J. B. Hofmann, G. S. Jenkins, J. Ishikawa, S. Nakatsuji, S. Das Sarma, and H. D. Drew, *Phys. Rev. B* **92**, 241108(R) (2015).
- [32] D. W. Berreman, *J. Opt. Soc. Am.* **62**, 502 (1972).
- [33] I. Abdulhalim, *J. Opt. A Pure Appl. Opt.* **1**, 655 (1999).
- [34] T. Tamaya, T. Kato, K. Tsuchikawa, S. Konabe, and S. Kawabata, *J. Phys.: Condens. Matter* **31**, 305001 (2019).
- [35] O. V. Bugaiko, E. V. Gorbar, and P. O. Sukhachov, *Phys. Rev. B* **102**, 085426 (2020).
- [36] R. E. Camley, *Surf. Sci. Rep.* **7**, 103 (1987).
- [37] J. Hofmann and S. Das Sarma, *Phys. Rev. B* **93**, 241402(R) (2016).
- [38] J. C. W. Song and M. S. Rudner, *Proc. Natl. Acad. Sci. USA* **113**, 4658 (2016).
- [39] R. F. Wallis, J. J. Brion, E. Burstein, and A. Hartstein, *Phys. Rev. B* **9**, 3424 (1974).
- [40] R. L. Stamps, B. L. Johnson, and R. E. Camley, *Phys. Rev. B* **43**, 3626 (1991).
- [41] K. W. Chiu and J. J. Quinn, *Nuovo Cimento B* **10**, 1 (1972).